Electronic transport in smectic liquid crystals

I. Shiyanovskaya and K. D. Singer
Department of Physics, Case Western Reserve University, Cleveland, Ohio 44106

R. J. Twieg, L. Sukhomlinova, and V. Gettwert
Department of Chemistry, Kent State University, Kent, Ohio 44242

(Received 4 July 2001; revised manuscript received 23 January 2002; published 10 April 2002)

Time-of-flight measurements of transient photoconductivity have revealed bipolar electronic transport in phenylnaphthalene and biphenyl liquid crystals (LC), which exhibit several smectic mesophases. In the phenylnaphthalene LC, the hole mobility is significantly higher than the electron mobility and exhibits different temperature and phase behavior. Electron mobility in the range $\sim 10^{-5}$ cm^2/V s is temperature activated and remains continuous at the phase transitions. However, hole mobility is nearly temperature independent within the smectic phases, but is very sensitive to smectic order, 10^{-3} cm^2/V s in the smectic-*B* (Sm-*B*) and 10^{-4} cm^2/V s in the smectic-*A* (Sm-*A*) mesophases. The different behavior for holes and electron transport is due to differing transport mechanisms. The electron mobility is apparently controlled by rate-limiting multiple shallow trapping by impurities, but hole mobility is not. To explain the lack of temperature dependence for hole mobility within the smectic phases we consider two possible polaron transport mechanisms. The first mechanism is based on the hopping of Holstein small polarons in the nonadiabatic limit. The polaron binding energy and transfer integral values, obtained from the model fit, turned out to be sensitive to the molecular order in smectic mesophases. A second possible scenario for temperature-independent hole mobility involves the competion between two different polaron mechanisms involving so-called nearly small molecular polarons and small lattice polarons. Although the extracted transfer integrals and binding energies are reasonable and consistent with the model assumptions, the limited temperature range of the various phases makes it difficult to distinguish between any of the models. In the biphenyl LCs both electron and hole mobilities exhibit temperature activated behavior in the range of 10^{-5} cm^2/V s without sensitivity to the molecular order. The dominating transport mechanism is considered as multiple trapping in the impurity sites. Temperature-activated mobility was treated within the disorder formalism, and activation energy and width of density of states have been calculated.

DOI: 10.1103/PhysRevE.65.041715 PACS number(s): 61.30.−v, 72.40.+w, 71.38.Ht, 72.10.−d

I. INTRODUCTION

Liquid crystals are an important class of organic materials that have been studied extensively due largely to their unique electro-optical characteristics and their applications in display devices [1–3]. However, and in contrast, the electronic transport properties of liquid crystals have only recently received attention. This current interest in the transport properties of liquid crystals stems from the numerous potential applications such as light-emitting diodes, photovoltaics, organic transistors, optical image processing, dynamic holography, and other molecular electronic and imaging devices, where the basic operation requires electronic charge generation and transport. Recent transport studies of columnar discotic liquid crystals based on the triphenylenes and other condensed aromatic hydrocarbons have shown fast electronic transport approaching that of the best organic crystals [4–7]. It has been demonstrated that the high degree of molecular organization in columnar discotic LCs plays an essential role in their high charge carrier mobility. These flat discotic molecules self-assemble into columns having a significant overlap of delocalized π electrons on adjacent molecules, thereby providing quasi-one-dimensional channels for facile charge transport. The simultaneous and substantial processing advantages and high charge mobility make LCs a promising media for applications. Recent studies by Funahashi and Hanna [8–11] have shown that smectic liquid crystals consisting of rodlike organic molecules (so-called ''calamitic'' LC) exhibit ambipolar transport with high charge mobility up to 10^{-2} cm^2/V s. The highly organized layer smectic structure provides for efficient carrier transport within the layers.

Electronic transport in organic materials is well described by a band model for organic single crystals and by a hopping formalism for disordered organic materials such as polymers, molecularly doped polymers, and glasses. Charge mobility in the band model is field independent. The hopping models consider charge motion as a continuous-time random walk between localized sites with isoenergetic positional disorder (the Sher-Montroll model [12]), as multiple trapping with energetic disorder of trapping sites [13,14], or as a hopping with a Gaussian distribution of energies and distances of the hopping sites (the Bässler disorder formalism [15–17]). The mobility due to the hopping mechanism is viewed as a thermally activated process of overbarrier jumps between localized hopping sites or tunneling through potential barriers (the Miller-Abrahams model [18]). As a result, hopping mobility is both field and temperature dependent.

LC materials, exhibiting orientational and two-dimensional (2D) positional order, represent an intermediate class of materials between single crystals and amorphous disordered materials. The charge transport mechanism in LCs is not well understood and no comprehensive charge transport

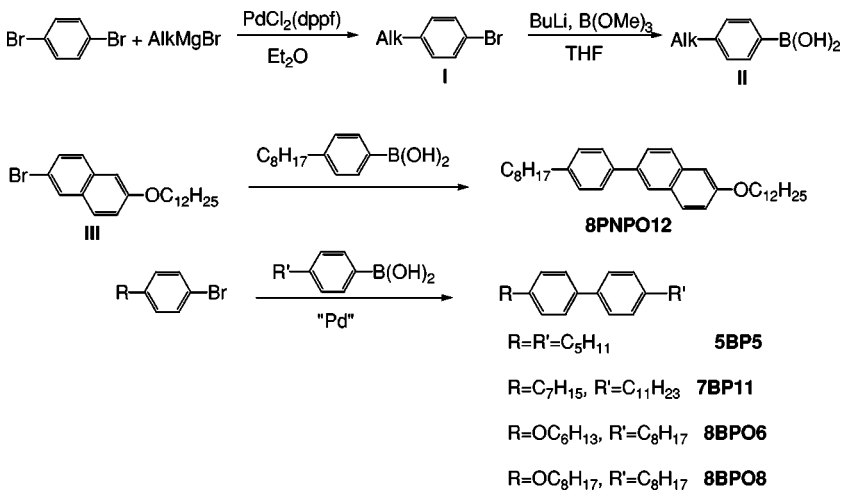

FIG. 1. General synthesis and molecular structures of the liquid crystal materials studied.

theory is presently available that describes the features of quasi-1D and-2D transport in LCs, including temperature- and field-independent mobility. A ''liquidlike'' structure in both discotic and smectic LCs is responsible for the dynamic nature of structural defects, which may serve as trapping sites. This is a key distinction in comparison with the static nature of charge traps in polymers and organic crystals. Because charge mobility is affected by trapping and detrapping processes, the self-healing character of positional disorder (the trapping sites) significantly increases charge mobility in LCs in comparison with polymers. Existing theoretical descriptions of charge transport in columnar discotic liquid crystals are based on hopping models with a static disorder approach developed for disordered molecular materials [6,7,19,20]. To the best of our knowledge, the only dynamic disorder approach examined thus far is based on the stochastic Haken-Strobl-Reineker model employed to treat hopping electronic charge transport in discotic triphenylene liquid crystals [21]. The transport properties of smectic LCs are an area of fast growing interest, but the limited temperature range for LC mesophases makes understanding the transport mechanism in dynamic quasi-two-dimensional systems challenging. One of the promising features of smectic LCs is that some materials can exhibit several smectic mesophases with different degrees of order and packing within the layers at different temperatures. Therefore, smectic LCs are a very convenient model system for understanding the relationship between molecular organization and photoelectric properties such as charge carrier photogeneration and transport under an applied electric field. Understanding the microscopic behavior of carrier transport in smectic liquid crystals can provide a protocol to design molecules with improved transport properties.

Since one expects a definite connection between molecular organization and charge transport, this paper is aimed at studying electronic transport in smectic LCs, which provide a variety of polymorphic structures ranging from a well-ordered crystal phase to a disordered isotropic liquid phase. Therefore, to establish transport mechanisms we have explored the field and temperature dependence of the electronic mobility in phenylnaphthalene and biphenyl smectic LCs, which exhibit several smectic phases with different levels of microscopic molecular organization. The mobility data for the phenylnaphthalene LC are compared with the preexisting data obtained by Funahashi and Hanna [10] for the same material synthesized by a slightly different procedure.

II. EXPERIMENTAL SECTION

A. Materials

1. Synthesis

The palladium catalyzed cross-coupling reaction between the 1-bromo-4-alkylbenzenes or 2-bromo-6-(dodecyloxy)naphthalene and an arylboronic acid (Suzuki coupling) represents the key step [22] of the overall liquid crystal synthesis as outlined in Fig. 1 The 1-bromo-4-alkylbenzenes (I) were prepared by palladium mediated coupling of 1,4-dibromobenzene with the appropriate Grignard reagent [23]. The arylboronic acids (II) were prepared by a standard method involving formation of aryllithium followed by trapping with trimethylborate and hydrolysis.

General procedure for Suzuki coupling: To a solution of a 1-bromo-4-alkylbenzene or 2-bromo-6-(dodecyloxy)naphthalene (4.4 mM) and $PdCl_2(PPh_3)_2$ or $PdCl_2$ (1 mol %) in benzene or toluene (7 ml) was added Na_2CO_3 (7 ml of a 2*M* solution in water), and the mixture was stirred for 15 min. The arylboronic acid (5 mM) dissolved in ethanol (7 ml) was then added and the reaction mixture was refluxed for 12 h. After this time the reaction mixture was cooled, extracted with ethyl acetate vs water, and the organic layer was dried over $MgSO_4$, filtered, and the solvent was removed *in vacuo*. All the crude liquid crystal products obtained in this fashion were subsequently purified by column chromatography (silica gel, petroleum ether) and then Kugelrohr (bulb to bulb) distillation. There appeared to be little correlation between the measured mobilities and the extent or exact combination of methods of purification. The transition temperatures and chemical structures of all liquid crystals after the indicated purification process are shown in Fig. 1.

2. General characterization

The ^{1}H NMR spectra were recorded on a Bruker AMX300 spectrometer. A polarized optical microscope equipped with a Mettler FP32 hot stage and Mettler FP5 temperature controller was used to observe the phase sequences and textures. A TA Instruments DSC 2920 differential scanning calorimeter was used to determine the phase transition temperatures. Heating and cooling rates were 2 °C/min. The details of general characterization and purification of the LC materials are shown in the Appendix.

B. Experiments

The LC cells were assembled from indium-tin oxide (ITO) coated glass substrates both with and without polyimide pretreatment. The cells were filled with the liquid crystals in the isotropic phase using the capillary effect, and then slowly cooled down to the LC mesophase with a cooling rate of about 0.1 °C/min. As a result, homeotropic alignment of the smectic layers with ''bookshelf'' geometry was achieved. Polarizing optical microscopy revealed a domain size in the range of 100 μm. The thickness of the empty cells was measured with a Perkin Elmer Lambda 18 UV/VIS spectrometer in the interference transmission mode. The cell thickness was adjusted with Mylar spacers ranged from 10 to 50 μm. The thickness of the LC layer was always much smaller than the domain size leading to conduction pathways free from domain boundaries. The dielectric constants of the LC materials were determined from capacitance measurements using a capacitance bridge and a lock-in amplifier.

The time-of-flight technique was employed to measure the transient photocurrent and to determine the mobility of charge carriers. The excitation source was a 3.6-ns *Q*-switched Nd:YAG (yttrium aluminum garnet) based laser that was frequency doubled and shifted using a H_2 stimulated Raman cell. The photoexcitation of the LC by laser irradiation ($\lambda = 320$ nm, third anti-Stokes component of a 532-nm pump) into the main absorption band of the LC resulted in the creation of electron-hole pairs in a very thin layer (light penetration depth less than 1 μm) near the illuminated electrode. Depending on the polarity of the applied electric field one charge carrier is eliminated at the illuminated electrode, while the other one moves through the sample towards the counter electrode. The charge motion creates a displacement current, which was measured with a current to voltage converter and preamplifier, and then was digitized with a Tektronix TDS3000 oscilloscope. The mobility was calculated using the well-known relation

$$\mu = l^2/\tau_T V, \tag{1}$$

where l is the thickness of the charge transport layer, τ_T is the transit time, and V is the applied voltage. According to the Sher-Montroll model, the transit time τ_T was defined as the intercept of the asymptotes of the pretransit and posttransit slopes of the photocurrent as plotted on a double logarithmic scale [12]. The dielectric relaxation time was always much higher than the experimental transit time, ensuring an absence of screening effects by bulk charges. The *RC* time constant of the cell and circuit was always much smaller than the transit time. The applied electric field was in the range of 2–20 V/μm and no changes in the LC alignment were observed at these fields. The pulse energy was adjusted using neutral density filters and kept below 3 μJ/pulse to prevent space charge buildup ensuring that the electric field is constant within the sample. The photogenerated charge was always two orders of magnitude smaller than the surface charge determined by the *CV* product. A beam splitter was used to monitor the intensity of the laser pulse. Samples were mounted in a Mettler hot stage with temperature maintained to 0.1 °C.

III. RESULTS AND DISCUSSION

A. Phenylnaphthalene (8PNPO12)

We have observed bipolar charge transport for all phases of 8PNPO12. Depending on the polarity of the applied electric field, holes or electrons transport through the sample resulting in photocurrent transients. When the illuminated electrode is positive biased, hole transport is observed, while negative bias produces electron transport. The magnitude of the electron photocurrents was always significantly smaller than that of the hole photocurrents in all the phases of this substance. The shape of the photocurrent transients provides information on the transport mechanism, and the shape was observed to depend on both the phase state of the compound and the polarity of the applied field. The 8PNPO12 compound exhibits two smectic mesophases Sm-*A* and Sm-*B* in the temperature range between the crystal phase and isotropic liquid state. In both smectic mesophases the molecules are arranged in layers with their molecular long axes on average perpendicular to the layer planes. The charge carrier transport occurs via the π-conjugated aromatic cores of the molecules, which thermally fluctuate in the smectic layers. Molecules in the least ordered Sm-*A* mesophase show no long-range positional order inside the layer and are able to rotate around the long molecular axes and to precess about the director. The Sm-*B* mesophase is characterized by long-range in-layer hexagonal packing of molecules, with motion limited to rotation about their long axes.

The time-of-flight photocurrent transients for the crystalline phase typically do not exhibit a characteristic plateau, but rather a featureless exponential decay with a slightly field-dependent time constant. The time constants were found to be approximately of 10^{-4} s and 10^{-5} s for hole and electron photocurrent decays, respectively. This featureless decay can be attributed to the deep trapping of the charge carriers at the crystallite grain boundaries. The lifetime of the deep traps is likely to be much larger than the transit time. By increasing the sample thickness up to 50 μm, we still could not reach a transit time comparable to the lifetime of the deep traps. Quantitative determination of the transit time for these dispersive transients was impossible even with a double logarithmic plot.

In the Sm-*B* mesophase, the charge carrier transport becomes much less dispersive, and differences in the shape of the photocurrent transients for both holes and electrons appear (Fig. 2). Figure 2(b) shows that the electron photocur-

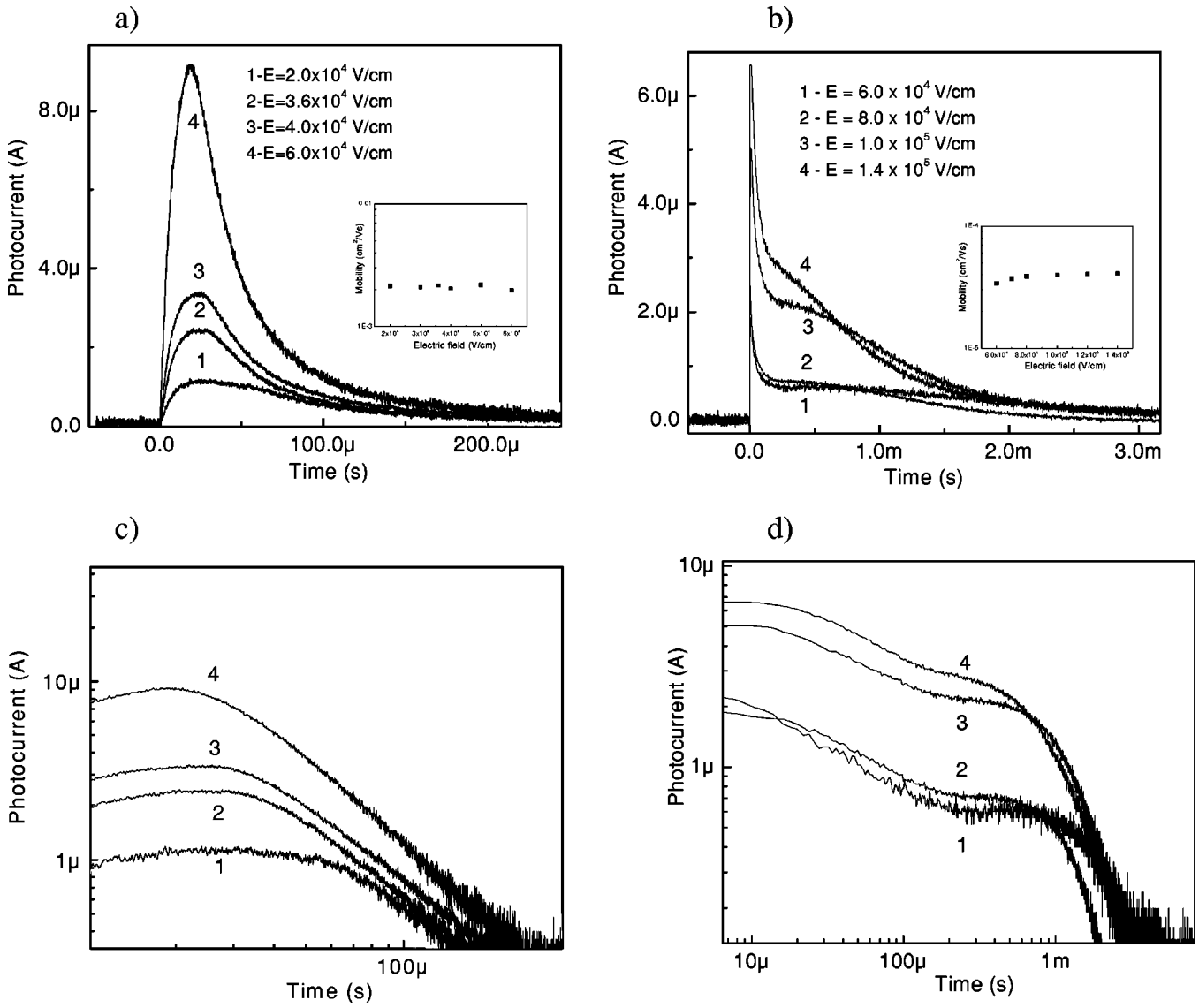

FIG. 2. Time-of-flight transients for 8PNPO12 in the smectic-*B* phase at 90 °C and at different values of the applied electric field: (a) and (b) linear plots of the hole and electron photocurrent transients, respectively; (c) and (d) double logarithmic presentation of the hole and electron photocurrent transients, respectively. The insets show the mobility vs the applied electric field. Intrinsic excitation by 320 nm wavelength (light intensity is 0.9 μJ/pulse). The cell thickness is 25.1 μm.

rents exhibit an initial short spike (usually tens of microseconds), a plateau region, and a long tail. This is a typical photocurrent shape observed for numerous molecular systems characterized by multiple trapping in shallow traps with charge carriers undergoing several trapping-detrapping events [17,24,25]. The initial spike is due to the trapping by sites with a lifetime exceeding the transit time in the sample, while the long tail is due to the dispersion of trap release times. As can be seen in Fig. 2(a), the hole photocurrents do not show the initial spike but exhibit a rise time, which becomes comparable to the transit time upon increase of the applied electric field. The existence of a rise time can be caused by carrier injection from the optically excited ITO layer [26] and/or by charge release from surface states. At higher electric fields, the time-of-flight transients become more dispersive due to a decrease in the transit time and its approach to the lifetime of the trapping sites. The mobility values were determined using a double logarithmic plot of the photocurrent transients and Eq. (1). The hole and electron mobilities were as high as 2.2×10^{-3} cm^2/V s and 3.3×10^{-5} cm^2/V s, respectively.

Typical photocurrent transients for holes and electrons in the Sm-*A* mesophase at 115 °C are shown in Fig. 3. Both carriers exhibit well-defined nondispersive transients with clear plateau regions, which are similar to those observed in columnar discotic liquid crystals [4–6]. The hole and electron mobility was determined to be 2.8×10^{-4} cm^2/V s and 4.3×10^{-5} cm^2/V s, respectively. Similar nondispersive time-of-flight transients for both charge carriers were obtained in the isotropic phase with mobilities of 1.8×10^{-4} cm^2/V s and 6.5×10^{-5} cm^2/V s for holes and electrons, respectively. The nondispersive nature of the carrier transport in the isotropic phase is due to short-range molecular order.

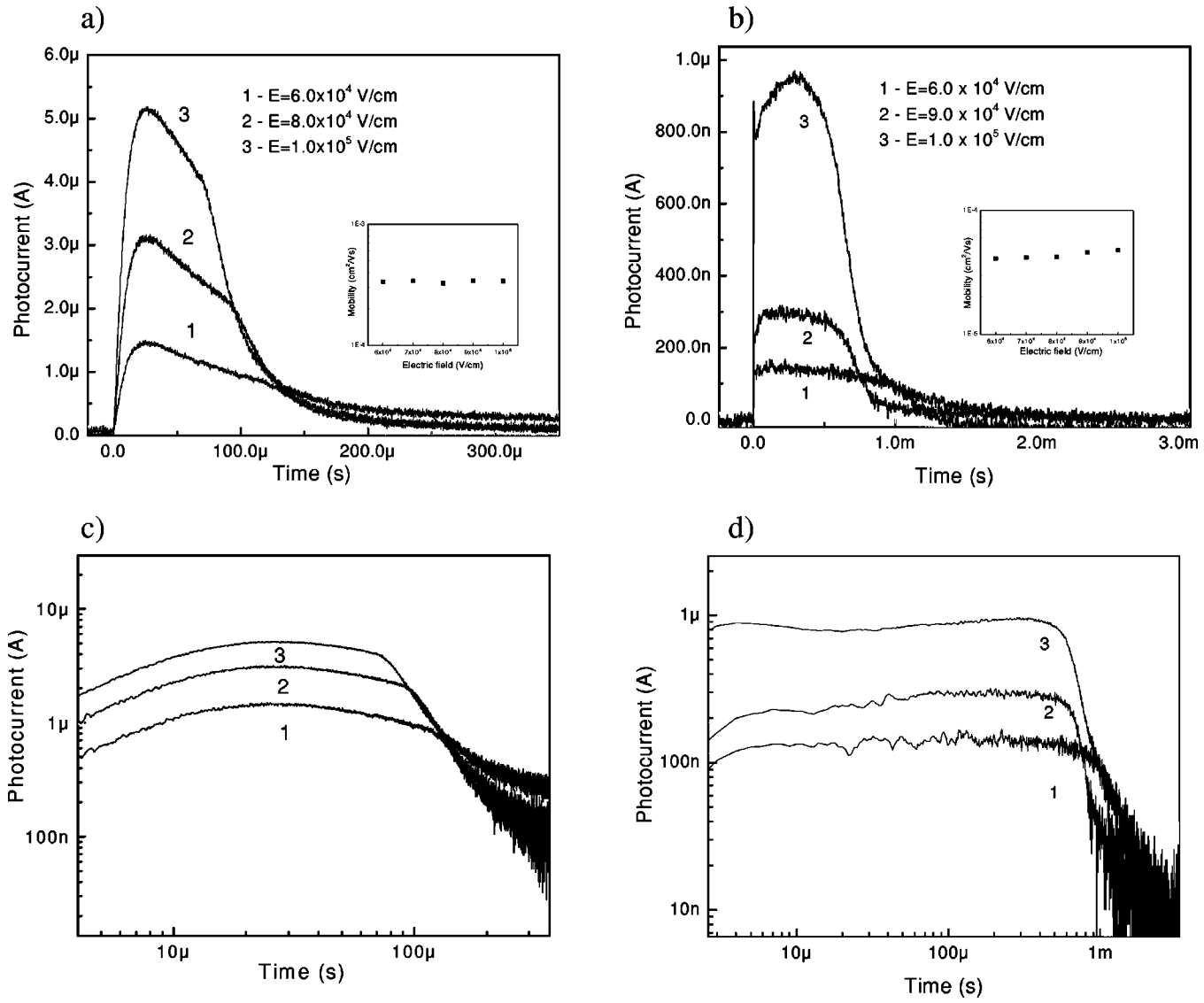

FIG. 3. Time-of-flight transients for 8PNPO12 in the smectic-*A* phase at 110 °C and at different values of the applied electric field: (a) and (b) linear plots of the hole and electron photocurrent transients, respectively; (c) and (d) double logarithmic presentation of the hole and electron photocurrent transients, respectively. The insets show the mobility vs the applied electric field. The cell and experimental conditions are the same as in Fig. 2.

Analysis of photocurrent transients reveals that the hole mobility does not exhibit temperature dependence and remains constant within the mesophase and undergoes an abrupt change at the phase transitions as demonstrated in Fig. 4(a). Contrary to the sensitivity of the hole mobility to the molecular ordering, the electron mobility increases slightly with temperature as seen in Fig. 4(b), without any notable dependence on the phase state. In addition, both the hole and electron mobilities were found to be field independent within smectic mesophases over the applied field range [insets in Figs. 2(a), 2(b), 3(a), and 3(b)]. Moreover, the mobility was thickness independent over the applied electric field range of 10^4-10^5 V/cm with transit time scaling as the square of the cell thickness.

Despite the weak temperature dependence of the mobility for negative carriers, which might appear to be thermally activated ionic diffusion, it is more likely that the electrons and no-negative ions are the active negative carriers. If the negative carrier mobility originates from ionic motion, a sharp increase in mobility would be expected at the transition from the viscous smectic phase to the nonviscous isotropic phase. Usually diffusion coefficients for ions change by several orders of magnitude upon the phase transition from viscous to nonviscous states. Moreover, the diffusion constant changes discontinuously even at phase transitions between different smectic orders. For example, diffusion constants within smectic layers for the C12-benzylideneamino-azobenzene compound are found to be 5×10^{-7} cm^2/s (120 °C) and 2.5×10^{-8} cm^2/s (115 °C) for Sm-*A* and Sm-*B*, respectively [27,28]. As can be seen in Fig. 4(b) the mobility of the negative charge carriers changes continuously at both the Sm-*B*/Sm-*A* and Sm-*A*–isotropic liquid phase transitions. Additionally, if we suppose that the negative carriers include both electrons and negative ions then we should ob-

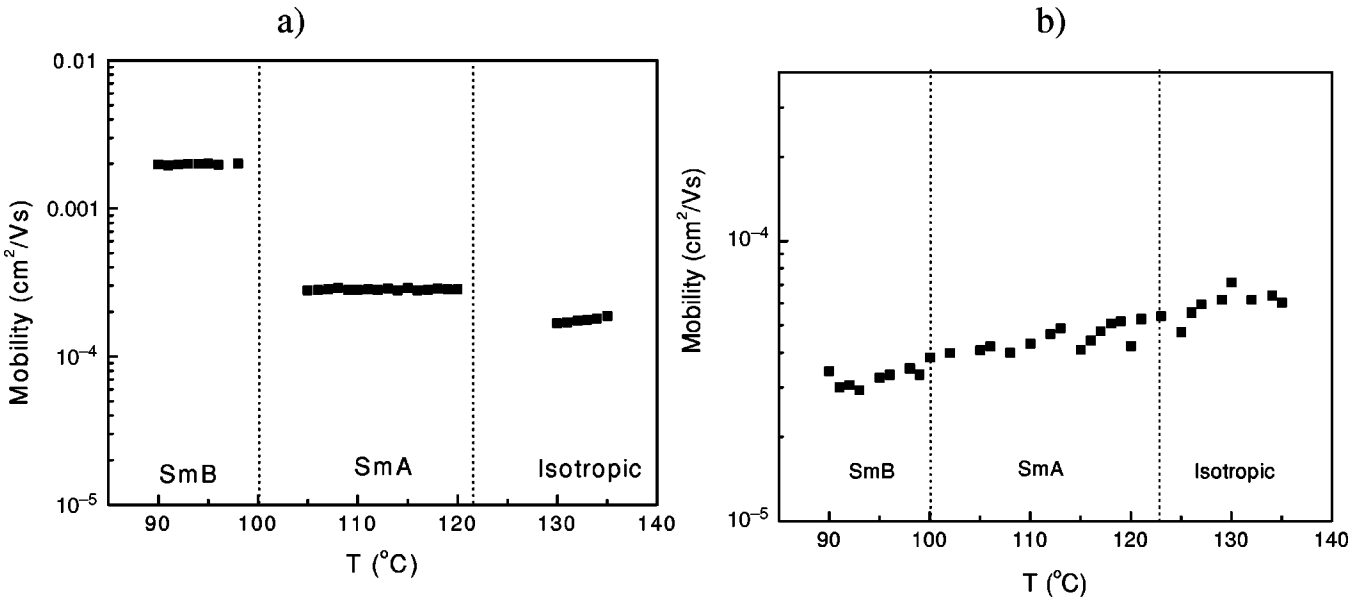

FIG. 4. Temperature dependence of the hole (a) and electron (b) mobilities for 8PNPO12. The cell and the experimental conditions are as in Fig. 2.

serve a separation in time between electron and ion transports due to the fact that the electrons have a significantly higher mobility than the negative ions. In fact, we did not observe the photocurrent transients with the features occurring in different time domains. Thus, negative charge photocurrents are most likely due to electron transport rather than ionic motion.

An interesting feature of the bipolar charge transport in 8PNPO12 is the different temperature dependence for hole and electron mobility, which is evidence for different transport mechanisms governing the hole and electron motion. Despite the fact that at low electric field, transport mechanisms of either multiple trapping or multiple hopping are indistinguishable [29], the different temperature dependence for hole and electron mobility permits identification of the transport mechanisms and rate-limiting factors for holes and electrons. The mechanisms for both charge carriers are characterized by jumps between neighboring molecules with distributions of distances and energy levels (static positional and energetic disorder) that fluctuate in time (dynamic disorder) in LCs. Thus, on a molecular level, holes and electrons are subject to similar positional and energetic disorder. At the same time, holes exhibit nondispersive time-of-flight transients and temperature-independent mobility, while the electron transport is dispersive with temperature-dependent mobility being one to two orders of magnitude smaller than that of holes. This allows us to assume that in addition to the multiple hopping, which both carriers experience under the influence of an applied electric field, there is an extra multiple trapping mechanism for electron transport only, most likely due to the impurity states exhibiting static disorder.

It should be noted that the mobility values for holes and the observed shapes of the hole photocurrent transients are in a good agreement with data reported by Funahashi and Hanna [8], who synthesized this material and studied its transport properties for the first time. However, the electron mobility is found to be two orders of magnitude less than that observed by Funahashi and Hanna's. The shape of the electron photocurrent transients allows us to assume that our compound contains some uncontrolled impurities, which introduce shallow electron trap sites in the transport manifold but do not significantly affect the hole transport states. Similar behavior was demonstrated, for example, in impurity effects in *a*-Se, which showed that arsenic doping significantly decreased the electron mobility while hole mobility was largely unaffected [30]. If we assume that the impurity has a higher ionization potential or HOMO (highest occupied molecular orbital), and a higher electron affinity or LUMO (lowest unoccupied molecular orbital), than that of the LC, then the HOMO levels of the impurity molecules do not serve as hole trapping sites and do not participate in hole transport. At the same time, the LUMO levels of the impurity are energetically preferable for moving electrons and act as traps, which inhibit the electron transport. It is of ultimate importance to understand the origin and nature of these impurities in order to measure the intrinsic mobilities and then tailor the electronic mobility. Materials exhibiting ambipolar transport characterized by fast and slow carriers simultaneously can be attractive for some device applications. For example, materials with low electron mobility and high hole mobility can be of importance for light-emitting diodes, which require good balancing of electron and hole currents and an efficient capture of charge carriers within the emissive layer. To efficiently capture carriers, it is necessary that one of the carriers have low mobility. This results in sufficiently high local charge density to ensure charge recombination and light emission [31].

As the electron transport is considered in terms of static disorder of distances and energies of the trapping site, the limited temperature range and weak temperature dependence do not allow for a unique choice of the temperature dependence for electron mobility. The observed temperature

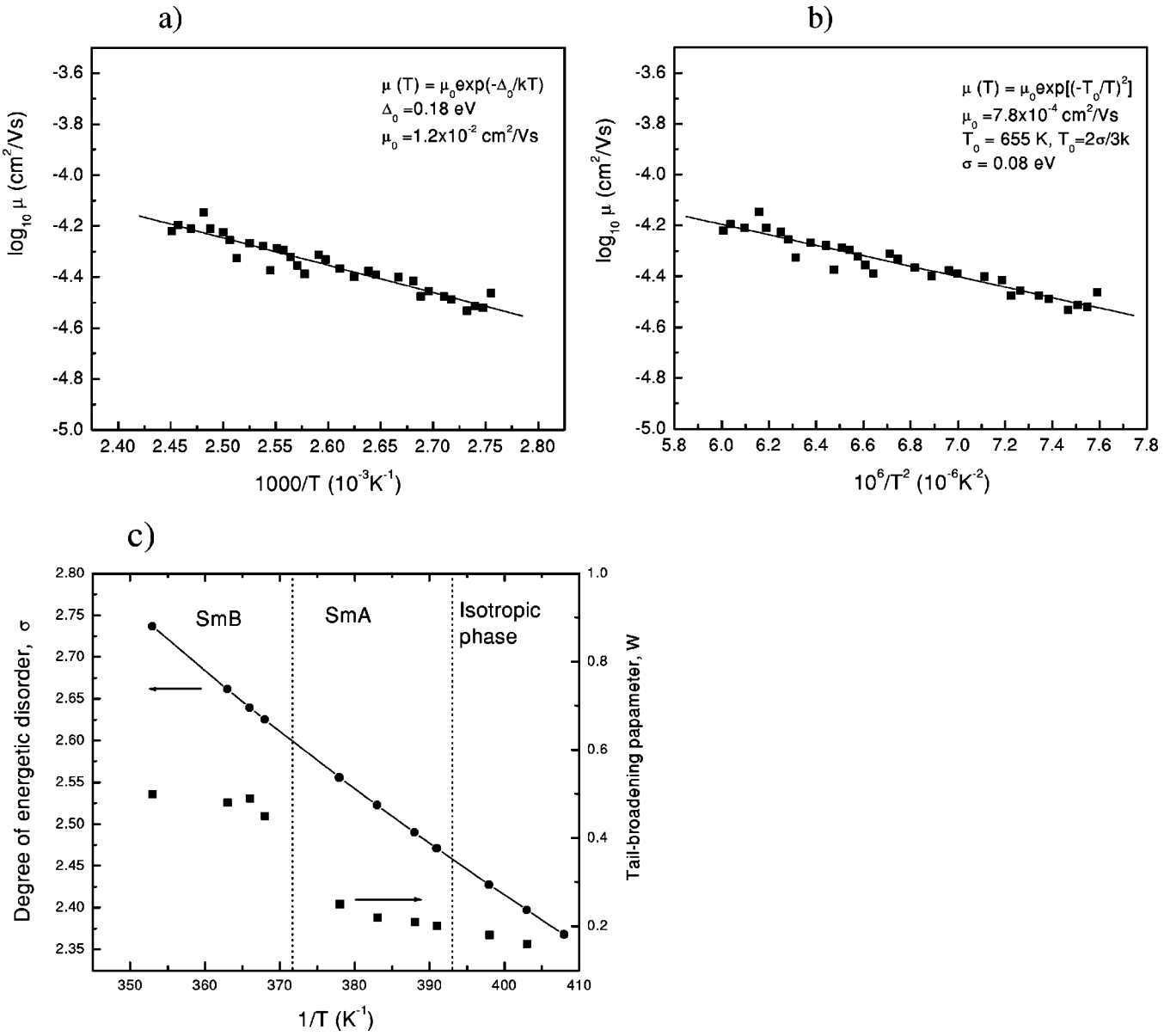

FIG. 5. Temperature dependence for the electron mobility in 8PNPO12: (a) in Arrhenius-type presentation $\log_{10}\mu$ vs T^{-1} and (b) in $\log_{10}\mu$ vs $1/T^2$ presentation. (c) Temperature dependences of the degree of energetic disorder for electron trapping sites $\hat{\boldsymbol{\sigma}}$, $\hat{\boldsymbol{\sigma}}=\sigma/kT$, and of the tail-broadening parameter W.

dependence can be fit by an Arrhenius-like law, $\mu=\mu_0\exp(-\Delta_0/kT)$, where Δ_0 is the activation energy, k is the Boltzmann constant, and μ_0 is the mobility at $T\rightarrow\infty$. This fit is shown in Fig. 5(a). The temperature dependence also can be treated by a $\mu=\mu_0\exp[-(T_0/T)^2]$ law, where $T_0=2\sigma/3k$ and σ is the width of the Gaussian density of energy states according to the Bässler disorder formalism. The corresponding fit is presented in Fig. 5(b). The Arrhenius plot yields an activation energy for the electron mobility of 0.18 eV, which corresponds to shallow trapping sites. The width of the Gaussian distribution of the density of states was determined from the plot $\ln\mu$ vs T^{-2} and found to be of 0.08 eV. The fitting parameters are summarized in Table I. The degree of energetic (diagonal) disorder of the trapping sites $\hat{\boldsymbol{\sigma}}$, defined as $\hat{\boldsymbol{\sigma}}=\sigma/kT$, is shown as a function of temperature for LC mesophases and the isotropic phase in Fig. 5(c). The disorder parameter decreases approximately from 2.7 for the Sm-*B* mesophase to 2.4 for the isotropic phase. From Figs. 2(b) and 3(b), one can observe that the photocurrent transients become less dispersive as the temperature increases due to the decrease in energetic disorder [Fig. 5(c)]. The width of the tail of the time-of-flight transients is due to the distribution of release times from the trapping sites, which can be described by the tail-broadening parameter W, defined as $W=(t_{1/2}-\tau_T)/t_{1/2}$, where $t_{1/2}$ is the time for the photocurrent to decay to its half value at transit time τ_T [32]. In the applied electric field range of 10^4–10^5 V/cm the parameter W was found to be a decreasing function with temperature, as shown in Fig. 5(c).

Thus, summarizing the above results we may conclude that the electron transport is governed by a rate-limited mul-

TABLE I. Parameters deduced from the fit of the experimental temperature dependence of the trap-limited mobility for the smectic LCs according to the disorder formalism for hopping transport (Ref. [17]). The parameters (activation energy Δ_0, prefactor mobility μ_0, and width of the Gaussian distribution of density of states, $\sigma = \frac{3}{2}kT_0$) were obtained from the data given in Figs. 5(a), 5(b), and 10 by fitting to equations $\mu = \mu_0 \exp(-\Delta_0/kT)$ and $\mu = \mu_0 \exp[(-T_0/T)^2]$.

		$\mu = \mu_0 \exp(-\Delta_0/kT)$		$\mu = \mu_0 \exp[(-T_0/T)^2]$		
Material	Charge carries	Δ_0 (eV)	μ_0 ($cm^2/V\,s$)	T_0 (K)	μ_0 ($cm^2/V\,s$)	σ (eV)
8PNPO12	Electrons	0.180	1.2×10^{-2}	655	7.8×10^{-4}	0.080
8BPO8	Electrons	0.108	4.2×10^{-4}	423	1.0×10^{-4}	0.053
8BPO8	Holes	0.106	4.5×10^{-4}	409	1.0×10^{-4}	0.051
8BPO6	Electrons	0.110	3.2×10^{-4}	462	9.0×10^{-5}	0.057
8BPO6	Holes	0.110	3.2×10^{-4}	447	9.0×10^{-5}	0.056

tiple trapping process. The localized trapping states are formed by impurity molecules with a higher LUMO level than that of LC molecules. These chemical traps exhibit a narrow Gaussian distribution of localized states (80 meV). Impurities may result in a distortion of the liquid crystalline order and the appearance of the structural defects as static traps.

As mentioned above, the hole mobility was both temperature and field independent within the smectic mesophase, which is inconsistent with carrier hopping models based on a field-assisted random walk between hopping sites with static positional and energetic disorder [16,24]. Discotic columnar liquid crystalline materials based on triphenylene derivatives also exhibit temperature- and field-independent hole mobility in the mesophase [4–6]. Their fast quasi-1D transport ($\mu \sim 10^{-1}$–10^{-4} $cm^2/V\,s$) was attributed to a strong overlap of π orbitals in the aromatic cores. One model considered the transport mechanism to be charge carrier hopping between neighboring molecules with a distribution of hopping rates due to a liquidlike disorder in columnar stacks, resulting in a fluctuation of intermolecular distance [33], but this should preclude temperature-independent mobility. For 1D transport in the columnar LC phase, Palenberg *et al.* [21] have advanced a hopping model based on pure dynamic disorder showing that temperature-independent charge transport could be achieved by assuming small fluctuations of the overlap integral between neighboring molecules. In the case of large fluctuations, the temperature dependence can be canceled over a restricted temperature range by differing contributions of rotational motion (around the columnar axis) and translational motion (along the columnar axis) of the molecules. However, the presence of static disorder would lead to a thermally activated process.

In order to explain the lack of temperature dependence in the mobility, it is reasonable to invoke hopping models that go beyond that of the bare carrier, such as polaron models. In this case, hopping in the presence of positional and energetic disorder is applied to carriers dressed with phonons. Temperature-independent mobility was also encountered for organic molecular crystals, e.g., such as naphthalene and anthracene [34–36]. Usually the charge transport in organic molecular solids is treated at low temperatures as a bandlike coherent carrier motion with a power law dependence $\mu(T) \propto T^{-n}$ $(n=0$–$3)$ [37]. At high temperatures, when the mean free path of the carriers becomes comparable with intermolecular distance, the band model does not hold and transport is described by the nearly small molecular polaron model developed by Silinsh and co-workers [38,39]. A nearly small molecular polaron is produced by localized charge carrier interacting with intramolecular vibrations. In accordance with the molecular polaron model, charge transport proceeds as nonthermally activated tunneling (coherent motion) between neighboring molecules with $\mu_{mp}(T) \propto T^{-n}$ dependence of the molecular polaron mobility μ_{mp}. The molecular polaron mobility is field independent up to sufficiently high electric fields, which can induce charge scattering on lattice phonons. To explain the temperature-independent mobility, Silinsh *et al.* have proposed competition between two different polaron-type mechanisms [40]. Along with a nearly small molecular polaron there is a small lattice polaron formed as a result of the interaction of the localized charge with intermolecular vibrations, which results in the formation of the induced dipoles on neighbor molecules. The neighboring molecules are displaced from equilibrium as a result of this charge-induced dipole interaction. The transport of small lattice polarons is a thermally activated hopping process (incoherent motion) with the characteristic dependence for mobility $\mu_{sp}(T) \propto \exp(-\Delta_{sp}/kT)$, where Δ_{sp} is the activation energy of the small polaron mobility μ_{sp}. The competition between these two mechanisms in the effective carrier mobility $\mu_{eff}(T)$ can result in the cancellation of the temperature dependence [40],

$$\mu_{eff}(T) = \mu_{mp} + \mu_{sp} = aT^{-n} + b \exp[-\Delta_{sp}/kT]. \quad (2)$$

In this model, the hole mobility data can be deconvoluted into two components: the nearly small molecular polaron mobility and the small lattice polaron mobility according to Eq. (2), the empirical approach developed by Karl [41]. The very narrow temperature range of the smectic mesophases results in multiple sets of parameters n and Δ_{sp} for the two mobility components. Nevertheless, reasonable parameter values (e.g., $n=2.1$ and $\Delta_{sp}=50$ meV for the Sm-*A* phase) can be deduced as a result of deconvolution. LC materials with a wider temperature range will be necessary to confirm this mechanism.

Another approach that can result in temperature-independent mobility is based on the two-site small polaron model developed by Holstein for 1D charge transport in molecular crystals [42,43]. In the nonadiabatic limit, when the nearest-neighbor transfer integral J between two hopping sites is much smaller then the polaron binding energy E_p, the Holstein polaron mobility is defined as [35,42–45]

$$\mu_p = \frac{1}{(kT)^{3/2}} \frac{ed^2}{h} \left(\frac{\pi}{2E_p} \right) J^2 \exp\left(-\frac{E_p}{2kT} \right), \tag{3}$$

where e is the elementary charge and d is the intermolecular distance. The transfer integral is a measure of the interaction energy between two neighboring molecules. An appropriate value of E_p can result in a cancellation of the temperature-dependent factors in Eq. (3). Further, liquid crystalline materials exhibit weak van der Waals intermolecular interactions, and it is reasonable to expect that J is small.

The applicability of a polaron approach to smectic LC can be considered if we suggest that hopping occurs between aromatic cores of neighboring molecules as was shown for discotic triphenylene materials [46]. The measured mobility and applied field allow for estimation of the mean hopping time Δt between molecules with intermolecular distance d, $\Delta t = d/\mu E$, where E is the applied electric field. The mean intermolecular distance for smectic LC is approximately 4 Å [10]. The estimated mean hopping time for an applied field in the range of 10^4–10^5 V/cm is 10^{-10}–10^{-9} s for holes in the Sm-*B* phase, 10^{-9}–10^{-8} s for holes in Sm-*A* and isotropic phases, and 10^{-8} s for electrons in all phases, taking into account that the upper limit of the characteristic relaxation times for both electronic and lattice polarization are smaller than 10^{-13} s, i.e., the polarization response of the local LC matrix is fast enough for the formation of a polaron-type quasiparticle around charge carriers localized at hopping sites. It has been shown recently by Kreouzis *et al.* [47] that temperature-independent mobility in two triphenylene columnar discotic liquid crystals can be successfully treated within the small polaron approach. It should be noted that field-independent hole mobility is a signature of bandlike transport. However, in order to consider hole transport to be bandlike, the mobility should be at least 1 $cm^2/V\,s$, which does not apply in the present case.

The fit of the experimental data for hole mobility given in Fig. 4(a) to the Holstein equation (3) is shown in Fig. 6 in the $\ln(\mu T^{3/2})$ vs T^{-1} representation. The polaron binding energy E_p was found to be 0.144 eV and 0.104 eV for the Sm-*B* and Sm-*A* phases, respectively. The transfer integral, which is inversely proportional to the time interval between hopping, was equal to 3 meV for the Sm-*B* mesophase and 1 meV for the Sm-*A* mesophase. The Holstein nonadiabatic regime holds when $J \ll E_p$. It can be seen that our data satisfy the above requirement and that the small polaron model is consistent with the observed hole transport behavior in smectic LC. The transfer integral for organic molecular crystals is usually less that 30 meV [35,36]. Because of molecular motion in the LC state, it is plausible to expect that the transfer integral should be smaller than that in molecular crystals.

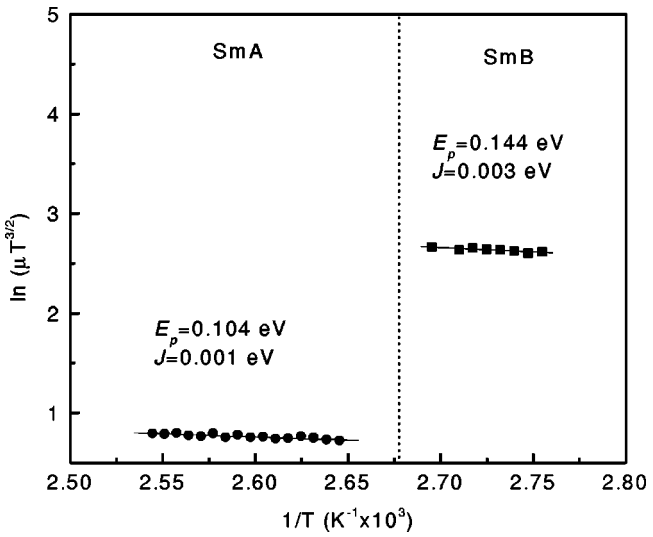

FIG. 6. Hole mobility data for 8PNPO12 in the $\ln(\mu T^{3/2})$ vs $1/T$ presentation. Solid lines are the fit to the Holstein small polaron model in the nonadiabatic limit given by Eq. (3).

Moreover, because the Holstein model is a one-dimensional model, quasi-2D transport in the smectic LC can result in a lower value of the transfer integral due to the possible molecular motion between the smectic layers.

The fastest hole transport was observed in the Sm-*B* mesophase of the 8PNPO12 compound. The hole mobility in the Sm-*A* and isotropic phases was found to be smaller by an order of magnitude than that in the Sm-*B* phase. The rate-limiting step in charge transport is likely to be due to the molecular orientation and the transfer integral (which is determined by intermolecular orbital overlap). The physical properties of the Sm-*B* phase are consistent with those of both liquid crystalline and solid states. It has been shown that molecules within the smectic layer do not have independent rotational disorder and rotation is completely synchronized and cooperative [48]. We might, therefore, anticipate that the highly ordered Sm-*B* mesophase with molecules undergoing a cooperative rotation exhibit a small waiting time between hops. For the Sm-*A* mesophase the average distance between molecules increases, as there is no correlation in the rotational motion of the molecules about their long axis. Moreover, the molecules can precess, which will decrease the mean overlap of electron orbitals and increase the hopping time between consecutive jumps of the charge carrier and thereby decrease the mobility. As expected, the transfer integral J, was found to be larger for the more ordered Sm-*B* phase in comparison with that of the Sm-*A* phase. Thus, it can be seen that mobility is sensitive to the transfer integral and is consistent with the Holstein small polaron approach.

In summary, it is evident from our data that the mechanism of intrinsic hole transport in the 8PNPO12 smectic liquid crystal is different from that for molecular disordered systems. The hole transport can be seen as a self-trapping of localized holes due to the surrounding polarization followed by polaron hopping between neighboring molecules. Electron transport is dominated by impurities forming shallow

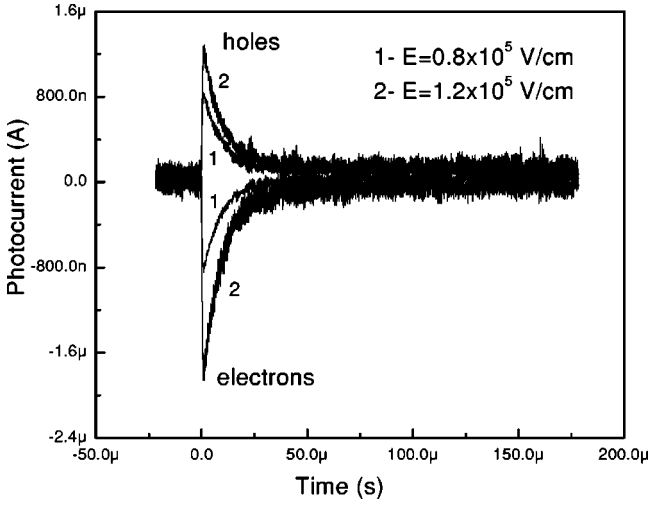

FIG. 7. Dispersive time-of-flight photocurrent transients for holes and electrons in the Sm-*B* mesophase of the biphenyl compound (7BP11) at different values of the applied field. Cell thickness is 25.3 μm, light intensity is 1.8 μJ/pulse, excitation wavelength is 320 nm.

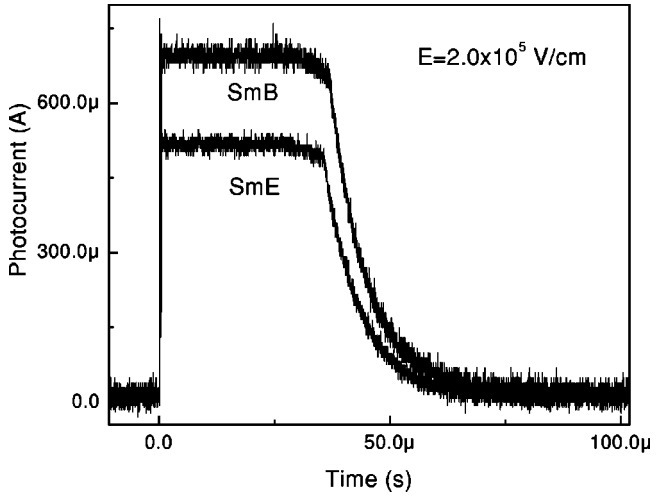

FIG. 8. Trap-free hole photocurrents in the Sm-*E* (409 °C) and Sm-*B* (50 °C) mesophases of the biphenyl compound (5BP5). Excitation wavelength is 320 nm, cell thickness is 25.6 μm.

trapping sites and can be considered within the disorder formalism developed for disordered molecular solids.

B. Biphenyls (7BP11 and 5BP5)

The molecules of two biphenyl compounds 7BP11 and 5BP5 have been studied to elucidate the charge transport in smectic mesophases formed by relatively small molecules. The 7BP11 material exhibits a Sm-*B* phase, while the 5BP5 compound shows two smectic mesophases, Sm-*B* and smectic-*E* (Sm-*E*). In the Sm-*E* mesophase molecules are arranged in long-range orthorhombic packing in the layer. Studies of dynamic motion in the Sm-*E* phase reveal that molecular rotation along the long molecular axis is strongly hindered. Contrary to the Sm-*B* phase, even cooperative rotation is not possible due to the very close molecular packing [49]. For both biphenyl materials we have observed a very fast exponential decay of the hole and electron photocurrents for all the crystal, smectic, and isotropic liquid phases. The decay time of the photocurrent transients was the same for film thicknesses in the range of 12–50 μm and over the applied field range of 10^4–10^5 V/cm. Typical time-of-flight transients for both holes and electrons for the 7BP11 compound in the smectic-*B* phase (55 °C) with 320 nm excitation and at the different values of the applied electric field are shown in Fig. 7. This behavior of photocurrent transients can originate from range limited transport. The carrier transport becomes range-limited when the carrier gets trapped after several hops for a sufficient period of time so that it does not participate in transport any longer. In this case, the generated carriers do not propagate over the entire sample, but immobilize at deep trapping sites in the vicinity of the carrier generation region. The nature of such deep traps is unknown and may be caused by impurities resulting from residual products of synthesis. The origin of range-limited transport is completely different from that of the dispersive transients where all generated carriers move through the sample and arrive at the counter electrode at different times due to the distribution of trap lifetimes. In the case of range-limited transport, the mobility cannot be determined from the time-of-flight transients.

The most striking feature of the charge transport in both the biphenyl compounds was the appearance of a giant photocurrent when the LC cell was repeatedly pulsed without grounding after the light pulse. Figure 8 shows this giant photocurrent for the Sm-*E* and Sm-*B* mesophases in the 5BP5 compound. The magnitude of the giant photocurrent was higher than that observed for the initial single light pulse by several orders of magnitude. The observed effect can be explained by the existence of deep trapping and an effect of residual charge trapped from the previous light exposures. The deep traps can be efficiently filled with each light pulse producing a significant space charge field. The emission-limited conditions are no longer valid and the system is space charge limited. In this mode the generated trap-free photocurrent becomes nonlinear in voltage and obeys Child's law. Appearance of this trap-free photocurrent was often followed by dielectric breakdown of the materials.

In summary, the existence of very deep traps for both holes and electrons result in range-limited photocurrents. The lifetime of the trapping sites is much longer than the transit time and, therefore, deep trapping can obscure the intrinsic transport mechanisms, which are believed to be polaronic. The charge carrier may participate in polaron hopping until it gets trapped once, and after that it does not transport through sample. To observe the intrinsic transport mechanisms, the biphenyl LC materials have to be purified significantly.

C. Biphenyl derivatives (8BPO6 and 8BPO8)

Two other biphenyl compounds 8BPO6 and 8BPO8 exhibiting different smectic mesophases have been studied. The 8BPO6 compound exhibits two smectic mesophases Sm-*E* and Sm-*B*, while only the Sm-*B* phase exists in the 8BPO8 material. These compounds with an oxygen atom in one of

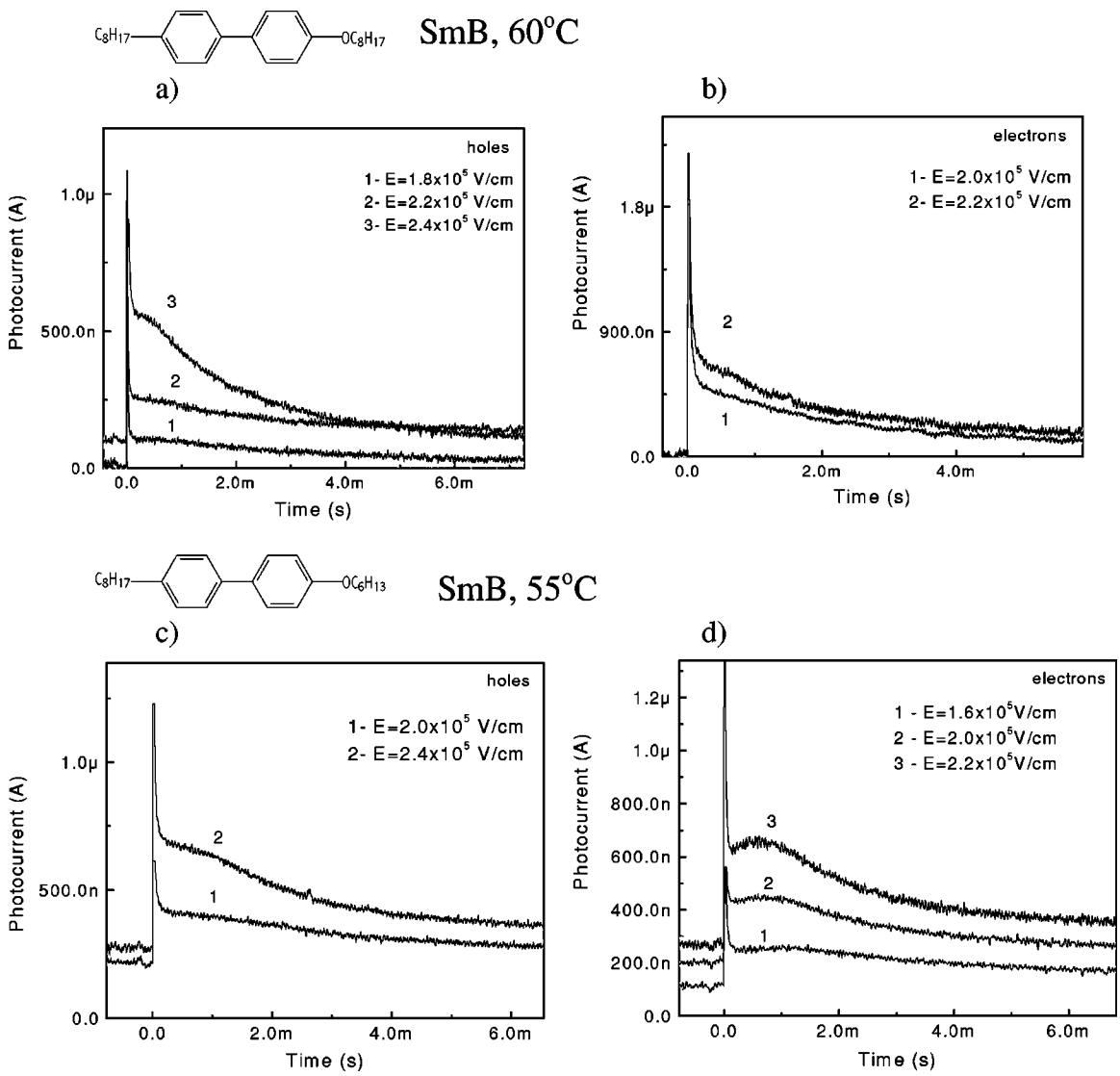

FIG. 9. Typical time-of-flight transients for the 8BPO8 (a),(b) and 8BPO6 (c),(d) liquid crystalline materials in the Sm-*B* mesophase. Cell thickness is 24.9 μm for the 8BPO8 compound and 25.2 μm for the 8BPO6 compound. Excitation wavelength is 320 nm, light intensity is 0.8 μJ/pulse.

the alkyl chains resulted in complete elimination of the very deep traps observed for the biphenyl 7BP11 and 5BP5 compounds. Photocurrent transients shown in Fig. 9 with well-developed plateau regions have been obtained for the 8BPO6 and 8BPO8 materials in the smectic mesophases. In both liquid crystalline materials the electron and hole mobilities have the same value in the range of 10^{-5} cm^2/V s. Both the electron and hole mobilities for the 8BPO6 liquid crystal were not sensitive to smectic order and slightly increased with temperature without any abrupt changes at the Sm-*E* Sm-*B* transition, as shown in Fig. 10(a). The mobility of both carriers was nearly field independent over the narrow applied field range [Fig. 10(b)]. The parameters obtained from fits of the temperature dependence of the mobility in the framework of the disorder formalism are shown in Table I. The temperature-activated behavior of both electron and hole mobilities with small activation energy Δ_0 ($\sim$100 meV) is likely to be due to multiple shallow trapping. Contrary to the 8PNPO12 compound, where only electrons are subject to impurity trapping, both carriers in the biphenyl derivatives appear to undergo trapping by impurity molecules.

Thus, temperature-activated hole and electron transport in the biphenyl derivatives is governed by multiple trapping in shallow traps. Because the lifetime of such trapping events is longer than polaron hopping time, multiple trapping mechanism is the rate-limiting factor and dominates over intrinsic polaron transport.

IV. CONCLUSIONS

By measuring transient photoconductivity, it was shown that the smectic LC material 8PNPO12 exhibits fast bipolar electronic transport. The mobility value, temperature dependence of the mobility, and sensitivity to the molecular organization were significantly different for hole and electron transport. Hole transport with high mobility, in excess of 10^{-3} cm^2/V s, is sensitive to smectic molecular order, which determines the hopping rate between neighbor molecules. We have suggested that hole transport can be considered as a

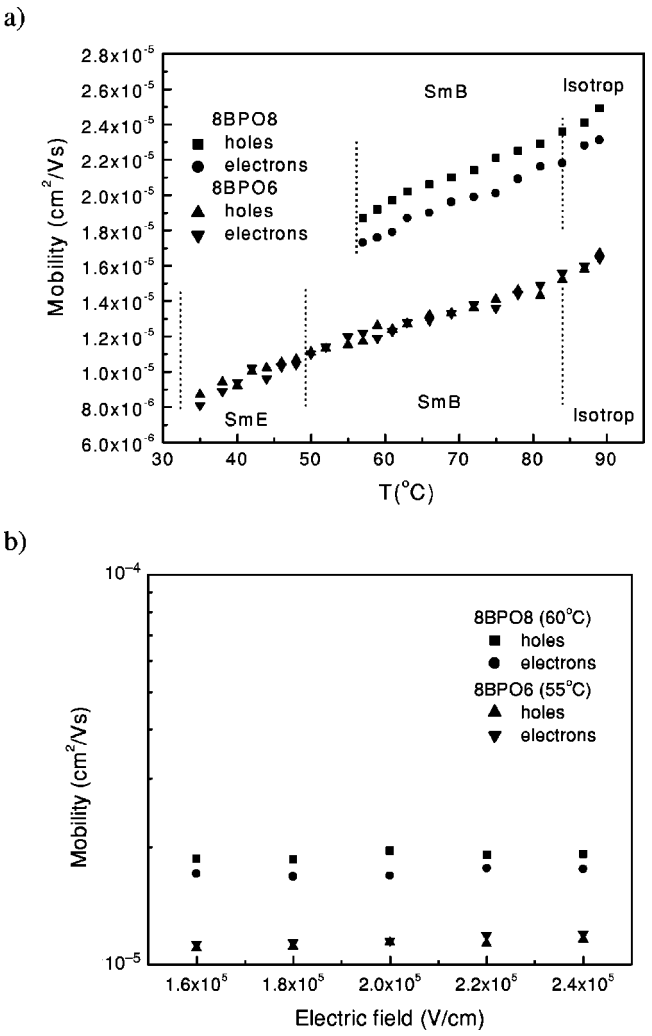

FIG. 10. Temperature (a) and field (b) dependences of the electron and hole mobilities for the biphenyl compounds 8BPO8 and 8BPO6. Experimental conditions are the same as in Fig. 9 with the applied electric field of 2.4×10^5 V/cm.

small polaron formed by localized carriers and induced electronic and molecular polarization, moving as a quasiparticle between hopping sites. We have shown that the temperature-independent mobility is consistent with the nonadiabatic limit of the Holstein small polaron model. It has been demonstrated that hole mobility is sensitive to the transfer integral that is determined by molecular orientation and motion in the smectic LC mesophases. Alternatively, the temperature-independent mobility can be explained by a competition between two coexisting polaron mechanisms: nearly small molecular polarons and small lattice polarons. Electron transport with a mobility of 10^{-5} $cm^2/V\,s$ is not sensitive to molecular orientation and is governed by shallow trapping due to impurities. The limited factor for electron transport is the lifetime of trapping sites. The temperature-activated electron mobility can be treated in the framework of the Bässler disorder formalism. Both the hole and electron mobilities are field independent over the narrow range of the applied electric field.

The biphenyl compounds 7BP11 and 5BP5 exhibit fast photocurrent decay due to the existence of very deep traps possibly due to impurities of an unknown nature. The biphenyl derivatives 8BPO6 and 8BPO8 show temperature-activated electron and hole mobility, which is governed by multiple shallow trapping and can be analyzed within the disorder model. It is believed that the existence of shallow or deep traps results in the disguise of the intrinsic transport mechanisms.

In summary, the temperature-independent mobility observed in this study suggests that the intrinsic transport mechanism in liquid crystalline materials is consistant with polaron hopping between sites with dynamical disorder. To test these and other models, experiments with smectic LC having wider temperature ranges should be performed. As was demonstrated, the purity of LC materials is a critical issue because impurity induced trapping can obscure the inherent fast transport in the LCs. In the case of shallow traps, the dominating transport is multiple trapping, while in the case of deep traps the carrier transport is range limited. In both the cases the intrinsic polaronic transport is obscured and is not evident in the time-of-flight experiments. A complete theoretical description of polarons in LC is still lacking and is of fundamental importance in order to understand the underlying transport mechanisms. The classical Holstein model and the Silinish model should be reconsidered to take into account quasi-2D transport in smectic liquid crystalline materials. The relationship between molecular organization and charge transport also requires further exploration.

ACKNOWLEDGMENTS

This work was supported by the Air Force Office of Scientific Research, Air Force Material Command, USAF (F49620-99-1-0018) and by the National Science Foundation through the ALCOM Science and Technology Center (DMR89-20147). Thanks are due to Professor J.-I. Hanna for helpful discussions and O. Ostroverkhova for technical assistance.

APPENDIX

2-Dodecyloxy-6-(4′-octylphenyl)naphthalene (8PNPO12) was purified in two different ways: (a) as described in Sec. II A 1 and (b) the Kugelrohr distilled material (230–260 °C/0.06 mm) was also recrystallized from petroleum ether, ^{1}H NMR ($CDCl_3$), chemical shift in ppm, δ, 0.89 (triplet, t, $3H$), 1.20–1.50 (multiplet, m, $31H$), 2.60–1.75 (m, $2H$), 1.80–1.90 (m, $2H$), 2.66 (t, coupling constant, $J=7.8$ Hz, 2H), 4.09 (t, $J=6.5$ Hz, $2H$), 7.14 (singlet, s, $1H$), 7.16 (doublet, d, $2H$), 7.28 (d, $2H$), 7.62 (d, $J=8.2$ Hz, $1H$), 7.75 (d, $J=9.0$ Hz, 1H), 7.78 (d, $J=8.6$, $2H$), 7.95 (s, $1H$). Transition temperatures, K (84.0) Sm-B (100.8) Sm-A (121.7) I; lit., K (79) Sm-B (100) Sm-A (121) I [8].

4,4′-Dipentylbiphenyl (5BP5) was purified by Kugelrohr distillation (200 °C/0.08 mm), ^{1}H NMR ($CDCl_3$), δ, 0.90 (t, $J=6.4$ Hz, $3H$), 0.91 (t, $J=6.4$ Hz, $3H$), 1.26–1.39 (m, $8H$), 1.60–1.70 (m, $4H$), 2.63 (t, $J=7.5$ Hz, $4H$), 7.25 (d,$J=8.3$ Hz, $4H$), 7.50 (d, $J=8.3$ Hz, $4H$). Transition temperatures (°C), K (28) Sm-E (48.8) Sm-B (56.2) I; lit., K (25.1) Sm-E (46.1) Sm-B (52.3) I [50].

4-Hexyloxy-4′-octylbiphenyl (8BPO6) was purified by Kugelrohr distillation (140–180 °C/0.11 mm) and subsequent recrystallization from hexane: ^{1}H NMR ($CDCl_3$), δ, 0.86–0.94 (m, $6H$), 1.28–1.90 (m, $20H$), 2.63 (t, $J=7.4$ Hz, $2H$), 4.00 (t, $J=6.5$ Hz, $2H$), 6.96 (d, $J=8.5$ Hz, $2H$), 7.23 (d, $J=8.0$ Hz, $2H$), 7.47 (d, $J=8.0$ Hz, $2H$), 7.51 (d, $J=8.5$ Hz, $1H$). Transition temperatures, K (32.0) Sm-E (48.6) Sm-B (82.3) I.

4-Octyloxy-4′-octylbiphenyl (8BPO8) was purified by Kugelrohr distillation (180–200 °C/0.14 mm): ^{1}H NMR (C_6D_6), δ, 0.91 (t, $J=6.8$, $6H$), 1.10–1.71 (m, $24H$), 2.58 (t, $J=7.5$ Hz, $2H$), 3.71 (t, $J=6.4$ Hz, $2H$), 6.50 (d, $J=8.7$ Hz, $2H$), 7.2 (d, $2H$), 7.51 (d, $J=8.0$ Hz, $2H$) 7.53 (d, $J=8.6$ Hz, $1H$). Transition temperatures, K (55.7) Sm-B (83.6) I; lit., K (57) Sm-B (86) I [51].

4-Heptyl-4'-undecylbiphenyl (7BP11) was purified by Kugelrohr distillation (170–190 °C/0.08 mm): ^{1}H NMR (C_6D_6), δ, 0.91 (t, $J=6.8$, $6H$), 1.10–1.71 (m, $24H$), 2.65 (t, $J=7.5$ Hz, $4H$), 7.30 (d, $4H$), 7.51 (d, $J=8.6$ Hz, $4H$). Transition temperatures, K (32.0) Sm-B (60.6) I.

[1] D. Demus, J. Goodby, G.W. Gray, H.-W. Spiess, and V. Vill, *Handbook of Liquid Crystals* (Wiley-VCH, Weinheim, 1998).

[2] *Physical Properties of Liquid Crystals*, edited by D. Demus, J. Goodby, G.W. Gray, H.-W. Spiess, and V. Vill (Wiley-VCH, Weinheim, 1999).

[3] S. Chandrasekhar and S.K. Prasad, Contemp. Phys. **40**, 237 (1999).

[4] D. Adam, F. Closs, T. Frey, D. Funhoff, D. Haarer, H. Ringsdoff, P. Schuhmacher, and K. Siemensmeyer, Phys. Rev. Lett. **70**, 457 (1993).

[5] D. Adam, P. Schuhmacher, J. Simmerer, L. Haussling, K. Siemensmeyer, K.H. Etzbach, H. Ringsdorf, and D. Haarer, Nature (London) **371**, 141 (1994).

[6] D. Adam, W. Romhildt, and D. Haarer, Jpn. J. Appl. Phys., Part 1 **35**, 1826 (1996).

[7] N. Boden, R.J. Bushby, J. Clements, B. Movaghar, K.J. Donovan, and T. Kreouzis, Phys. Rev. B **52**, 13 274 (1995).

[8] M. Funahashi and J.-I. Hanna, Appl. Phys. Lett. **71**, 602 (1997).

[9] M. Funahashi and J.-I. Hanna, Phys. Rev. Lett. **78**, 2184 (1997).

[10] M. Funahashi and J.-I. Hanna, Appl. Phys. Lett. **73**, 3733 (1998).

[11] M. Funahashi, and J.-I. Hanna, Appl. Phys. Lett. **76**, 2574 (2000).

[12] H. Sher and E.W. Montroll, Phys. Rev. B **12**, 2455 (1975).

[13] J. Noolandi, Phys. Rev. B **16**, 4466 (1977).

[14] F.W. Schmidlin, Phys. Rev. B **16**, 2362 (1977).

[15] H. Bässler, Phys. Status Solidi B **107**, 9 (1981).

[16] H. Bässler, Philos. Mag. B **50**, 347 (1984).

[17] H. Bässler, Phys. Status Solidi B **175**, 15 (1993).

[18] E. Miller and E. Abrahams, Phys. Rev. **120**, 745 (1960).

[19] A.M. van de Craats, L.D.A. Siebbles, I. Bleyl, D. Haarer, Y.A. Berlin, A.A. Zharikov, and J.M. Warman, J. Phys. Chem. B **102**, 9625 (1998).

[20] N. Boden, R.J. Bushby, J. Clements, K.J. Donovan, B. Movaghar, and T. Kreouzis, Phys. Rev. B **58**, 3063 (1998).

[21] M.A. Palenberg, R.J. Silbey, M. Malagoli, and J.-L. Bredas, J. Chem. Phys. **112**, 1541 (2000).

[22] N. Miyaura and A. Suzuki, Chem. Rev. **95**, 2457 (1995).

[23] N.A. Bumagin, E.V. Luzikova, and I.P. Beletskaya, Russ. J. Org. Chem. **31**, 1650 (1995).

[24] P.M. Borsenberger, E.H. Magin, M. van der Auweraer, and F.C. de Schryver, Phys. Status Solidi A **140**, 9 (1993).

[25] E. Muller-Hoersche, D. Haarer, and H. Sher, Phys. Rev. B **35**, 1273 (1987).

[26] H. Zong and J. Hanna, J. Appl. Phys. **88**, 270 (2000).

[27] G.J. Kruger, Phys. Rep. **82**, 229 (1982).

[28] M. Hara, S. Ichikawa, H. Takezoe, and A. Fukuda, Jpn. J. Appl. Phys., Part 1 **23**, 1420 (1984).

[29] B. Hartenstein, H. Bässler, A. Jakobs, and K.W. Kehr, Phys. Rev. B **54**, 8574 (1996).

[30] J.L. Hartke, Phys. Rev. **125**, 1177 (1962).

[31] R.H. Friend *et al.*, Nature (London) **397**, 121 (1999).

[32] L.B. Schein, Philos. Mag. B **65**, 795 (1992).

[33] N. Boden, R.J. Bushby, A.N. Cammidge, J. Clements, and R. Luo, Mol. Cryst. Liq. Cryst. Sci. Technol., Sect. A **261**, 251 (1995).

[34] E.A. Silinsh, *Organic Molecular Crystals. Their Electronic States* (Springer-Verlag, Berlin, 1980).

[35] M. Pope and C.E. Swenberg, *Electronic Process in Organic Crystals and Polymers* (Oxford University Press, Oxford, New York, 1999).

[36] E.A. Silinsh and V. Cápek, *Organic Molecular Crystals. Interaction, Localization, and Transport Phenomena* (AIP, New York, 1994).

[37] N. Karl, *Organic Semiconductors*, Landolt-Börnstein, New Series, Group III, Vol. 17, Pt. i (Springer, Berlin, 1985), pp. 106–218.

[38] E.A. Silinsh and A.J. Jurgis, Chem. Phys. **94**, 77 (1985).

[39] E.A. Silinsh, A.J. Jurgis, and G.A. Shlihta, J. Mol. Electron. **3**, 123 (1987).

[40] E.A. Silinsh, G.A. Shlihta, and A.J. Jurgis, Chem. Phys. **138**, 347 (1989).

[41] N. Karl, in *Proceedings of the 11th Molecular Crystal Symposium* (Lugano, Switzerland, 1985), p. 135.

[42] T. Holstein, Ann. Phys. (N.Y.) **8**, 325 (1959).

[43] T. Holstein, Ann. Phys. (N.Y.) **8**, 343 (1959).

[44] N. Mott, *Conduction in Non-Crystalline Materials* (Oxford Science, Oxford, 1997).

[45] B. Movaghar, J. Mol. Electron. **3**, 183 (1987).

[46] N. Boden, R.C. Borner, D.R. Brown, R.J. Bushby, and J. Clements, Liq. Cryst. **11**, 325 (1992).

[47] T. Kreouzis, K.J. Donovan, N. Boden, R.J. Bushby, O.R. Lozman, and Q. Liu, J. Chem. Phys. **114**, 1797 (2001).

[48] G.W. Gray and J.W.G. Goodby, *Smectic Liquid Crystals* (Leonard Hill, Glasgow, 1984).

[49] A.J. Leadbetter, J.C. Frost, and M.A. Mazid, J. Phys. (Paris) **40**, 325 (1979).

[50] K. Czuprynski, Liq. Cryst. **16**, 399 (1994).

[51] S.M. Kelly and J. Fünfschilling, Liq. Cryst. **20**, 77 (1996).